Available online at www.sciencedirect.com

ScienceDirect

journal homepage: http://www.elsevier.com/locate/rpor

Original research article

Evaluation of energy deposition and secondary particle production in proton therapy of brain using a slab head phantom

Sayyed Bijan Jia[a,1], *Mohammad Hadi Hadizadeh*[a,1], *Ali Asghar Mowlavi*[b,*], *Mahdy Ebrahimi Loushab*[a,1]

[a] *Physics Department, School of Sciences, Ferdowsi University of Mashhad, P.O. Box 91775-1436, Mashhad, Iran*
[b] *Physics Department, School of Sciences, Hakim Sabzevari University, P.O. Box 397, Sabzevar, Iran*

ARTICLE INFO

Article history:
Received 14 May 2013
Received in revised form
24 March 2014
Accepted 7 April 2014

Keywords:
Proton therapy
Slab head phantom
Bragg peak
Energy deposition
Secondary particle production

ABSTRACT

Aim: Evaluation of energy deposition of protons in human brain and calculation of the secondary neutrons and photons produced by protons in proton therapy.

Background: Radiation therapy is one of the main methods of treating localized cancer tumors. The use of high energy proton beam in radiotherapy was proposed almost 60 years ago. In recent years, there has been a revival of interest in this subject in the context of radiation therapy. High energy protons suffer little angular deflection and have a well-defined penetration range, with a sharp increase in the energy loss at the end of their trajectories, namely the Bragg peak.

Materials and methods: A slab head phantom was used for the purpose of simulating proton therapy in brain tissue. In this study simulation was carried out using the Monte Carlo MCNPX code.

Results: By using mono energetic proton pencil beams, energy depositions in tissues, especially inside the brain, as well as estimating the neutron and photon production as a result of proton interactions in the body, together with their energy spectra, were calculated or obtained. The amount of energy escaped from the head by secondary neutrons and photons was determined.

Conclusions: It was found that for high energy proton beams the amount of escaped energy by neutrons is almost 10 times larger than that by photons. We estimated that at 110 MeV beam energy, the overall proton energy "leaked" from the head by secondary photons and neutrons to be around 1%.

* *Corresponding author*. Tel.: +98 571 4411161; fax: +98 571 4411161.
E-mail addresses: bijan.Jia@stu-mail.um.ac.ir (S.B. Jia), mhhadi@ferdowsi.um.ac.ir (M.H. Hadizadeh), amowlavi@sttu.ac.ir, aa_mowlavi@yahoo.com, amowlavi@hsu.ac.ir (A.A. Mowlavi), ebrahimi.mahdy@gmail.com (M.E. Loushab).
[1] Tel.: +98 511 879 7022.
http://dx.doi.org/10.1016/j.rpor.2014.04.008

1. Background

Nowadays, radiation therapy is one of the three main methods of treating localized cancer tumors. Photons are the most common type of particles in radiotherapy.[1] Despite major technical developments,[2] the exponential decrease in the number of primary photons remains the main problem due to the nature of photon interactions in matter. Thus, photons have no well-defined range and their dose profiles diminish exponentially. So, a considerable dose is received by healthy organs, before and after the tumor. Unlike photons, charged particles have relatively well-defined penetration range. The dominant mechanism by which charged particles lose their energies is inelastic interaction with the atomic electrons. They lose most of their energies near the end of their paths, at the so called Bragg peak.[3,4]

Beside coulomb interaction with atomic electrons and elastic nuclear scattering, protons moving inside the matter undergo inelastic nuclear interactions in which secondary particles, such as neutrons, photons, secondary protons, deuterons, are produced.[3] In the energy range used for proton therapy, neutrons and photons are the most important secondary particles, in a sense that they can travel far distances from the target tissue and store their energies in other organs, thereby increasing the risk of secondary cancers.[5,6]

Secondary particles in hadron therapy have two different origins:

- First, those produced in the delivery system placed before particles enter the body. These can mostly be avoided by proper shielding.
- Second, those produced inside the body itself due to the interactions of incident particles with the body tissues, which cannot be eliminated with mechanical techniques. Therefore, their flux and energy deposition have to be calculated in order to estimate the risk of secondary cancers.

Quite numerous studies, with both Monte Carlo (MC) and experimental methods, have dealt with this issue.[6–10] Measured neutron doses from clinical proton facilities vary greatly, partly as a result of different measurement techniques, and partly as a result of different beam geometries.[11]

Kim et al.[12] compared secondary radiation doses from IMRT and proton beam therapy for lung and liver cancers using ion chamber and CR-39 detectors. They declared that the secondary dose per treatment Gy for proton beam therapy ranges from 0.17 to 0.086 mGy at 20–50 cm from the isocenter, whereas, it ranges from 5.8 to 1.0 mGy for IMRT. The internal neutron dose is much lower, ranging from 0.03 to 0.008 mGy. The dose due to the secondary neutrons and photons was estimated with Monte Carlo simulation for three existing proton therapy facilities by Agosteo et al.[10] They indicated that the dose from secondary particle for passive systems is 10 times higher than that for active systems. Paganetti et al.[6] used the Geant4 toolkit to simulate the proton beam line at MGH proton therapy center in order to estimate neutron doses to organs which are out-of-field. They divided the neutron dose into internal part, due to proton interactions in the body, and external part, due to proton interactions with components of the delivery system. Brenner and Hall[11] estimated neutron equivalent doses to relevant organs, based on the neutron doses reported by Paganetti et al., considering a conservative estimate of 25 for low-dose RBE. Then, they used these organ-specific equivalent doses to calculate lifetime cancer risks, using standard techniques which were described in the US National Academy of sciences BIER-VII report, and other radiation risk reports.[13–15] They estimated the overall lifetime cancer risk for a 15-year-old boy at about 4.7% and for a 15-year-old girl at about 11.1%. They indicated it to be larger for a younger patient and smaller for an older patient.

2. Aim

In this study we evaluated the energy deposition of the proton beam in the human brain phantom, and calculated the secondary neutrons and photons produced by protons. A good knowledge on pristine depth and lateral dose profiles in the target volume is necessary to choose a reasonable beam displacement to have a good conformation with the shape of the tumor, and spare the normal tissues.[16] Traditionally, dose calculations and TPS (treatment planning systems) in hadron therapy are, mostly, done in water[17] due to its proximity to soft tissues. To be more precise, it would be better to take into account the exact composition and sequence of different tissues.[18] This, indeed, is the main task of this work.

3. Materials and methods

3.1. *Head phantom*

The simplified head phantom was modeled. The tissue properties, from up to down, in vertical direction are 0.2 cm human skin, 0.3 cm soft tissue, 0.9 cm cranium, 11.5 cm brain, 0.9 cm cranium, and, finally, 0.5 cm soft tissue as presented in Fig. 1. Mass densities and compositions of the organs are given in Table 1.[19]

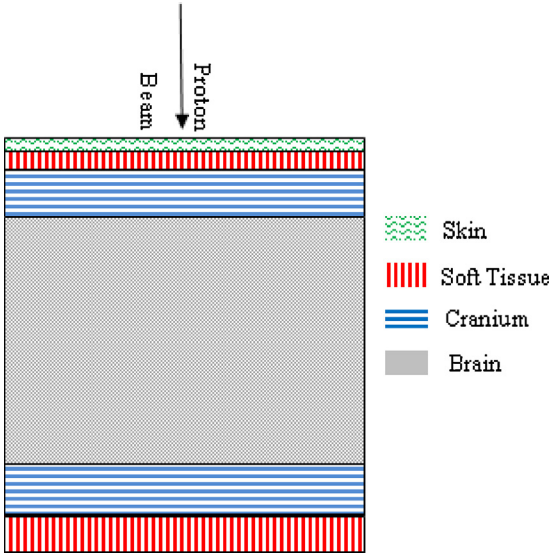

Fig. 1 – Geometry of the slab head phantom.

Table 1 – Mass density and elemental composition of the tissues in the head phantom (compositions are expressed as percentage by weight[19]).

Tissue type	Density (g/cm^3)	H	C	N	O	Ca	Na	P	S	Cl	K
Skin	1.09	10	20.4	4.2	64.5	–	0.2	0.1	0.2	0.3	0.1
Soft tissue	1.03	10.5	25.6	2.7	60.2	–	0.1	0.2	0.3	0.2	0.2
Cranium	1.61	5	21.2	4.0	43.5	17.6	0.1	8.1	0.3	–	–
Brain	1.04	10.7	14.5	2.2	71.2	–	0.2	0.4	0.2	0.3	0.2

Here, the lateral dimensions of the phantom were considered in accordance with the maximum values of the brain in the MIRD-ORNL phantom as 17.2 cm × 13.2 cm.[20] Mono energetic proton pencil beams perpendicular to the layers and toward the bottom of phantom were used, as showed in Fig. 1.

3.2. *Beam configuration*

PBS (pencil beam scanning) system requires less material in the beam line; range modulator wheel, patient-specific aperture, and compensator are not required. This substantially reduces the secondary particle production in the beam line. Thus, for pencil beam scanning systems the major source of secondary particles is the interaction of primary protons inside the patient, and not in the delivery system.[21] As the goal of this study, we investigated the energy deposition and secondary particle production inside the head phantom, we considered a simple pencil beam that is the outlet of a typical spot scanning delivery system. Here, we concentrated only on the interaction of the proton beam with the body tissues, and, therefore, the real beam line configuration did not matter. The beam in accordance with some active beam line facilities[3,22,23] is considered to have 7 mm of FWHM at the skin surface.

The energy deposition and also absorbed dose were calculated in various tissues of the slab head phantom for different energy beams with the goal that the proton Bragg peaks fall inside the brain tissue. The method of changing the beam energy depends on how the proton beam is generated. If a synchrotron is used, the energy can be changed dynamically, whereas in cyclotrons, energy may be changed by employing an energy selection system that is a set of energy degraders with different thicknesses. The ratio of the Bragg peak in depth dose profiles depends on the method used to change the beam energy. In the latter, some of the particles are removed from the beam as a result of scattering in the mechanical rang-shifters; for peaks with smaller depth, corresponding to thicker degraders, the height decreases; whereas, for the former, any increase in energy causes the energy and the range straggling to increase. Therefore, the width of the Bragg peaks increases for deeper seated peaks and, as a result, the height decreases. We considered a system in which the beam energy was changed dynamically. Using a mathematical algorithm, with the pristine dose profiles obtained from simulations for different beam energies as its input, the weight for each pristine peak was calculated in such a way that the spread out Bragg peak (SOBP) was reproduced longitudinally, and a flat dose distribution in the depth of the target volume was generated. Acquiring proper weight for each pristine peak is based on solving a set of linear equations explained by authors, in a yet-to-be-published work, to design a range modulator for a passive beam line. For a better conformation of the dose distribution with the target tumor, and sparing critical tissues in its proximity, it is essential to have the precise results for pristine depth dose profiles and the width of each peak. Our calculations show that to have a nearly uniform dose distribution in the tumor region using a typical spot scanning system, the beam displacement, both in traverse and depth, should be linked to the beam energy or, in other words, to the peak position.[24] For example, if the center of a typical tumor is placed 2 cm deep inside the brain, corresponding to the peak position of 70 MeV protons, to have a good modulation along the depth, the adjacent layers should be 0.5 mm apart (the average standard deviation of peak positions affect the modulated profile). If the tumor is located in a depth corresponding to 100 MeV protons, this distance should be 1.2 mm (average standard deviation of the peaks) to have uniform SOBP without ripples in dose distribution.

Secondary particles produced in the body of the patient, can impact the organs near the target region, and contribute substantially to the equivalent dose, whereas, those created in the delivery beam line, influence the whole body and affect the effective dose.[25] The secondary photon and neutron productions were studied along with the amount of energy escaped with these particles from the head. These are the main sources of secondary particles in the organs near the target volume in a typical scanning system. Finally, the energy spectra of these particles were determined.

3.3. *MCNPX*

The Monte Carlo simulations were performed using MCNPX (Monte Carlo N-Particles eXtension) code version 2.4 which is a modern, general-purpose Monte Carlo code developed at Los Alamos National Laboratory in USA.[26] MCNPX is the extension of MCNP code which is capable of tracking nearly all particles at nearly all energies. MCNPX utilizes the latest nuclear cross section libraries and uses physics models for particle types and energies where tabular data are not available. Several tally cards can be used to score different physical quantities. The tally results are tabulated in the pair of mean and relative errors.[27]

In the MCNPX, the energy of the residual nuclei and the non-traced particles are considered to be deposited locally at the point of production. To have more accurate results, one should track all particles that are predicted to be produced. In our simulations, protons, neutrons, photons, deuterons, tritons, helium-3 ions, and alpha particles were transported.

As for the cutoff energies, for being as precise as possible, they were set to the minimum values that can be traced in MCNP, i.e.; 1 MeV for protons, and 1 keV for electrons, positrons, and photons. As soon as a particle's energy falls below the cutoff, the transport simulation is terminated and

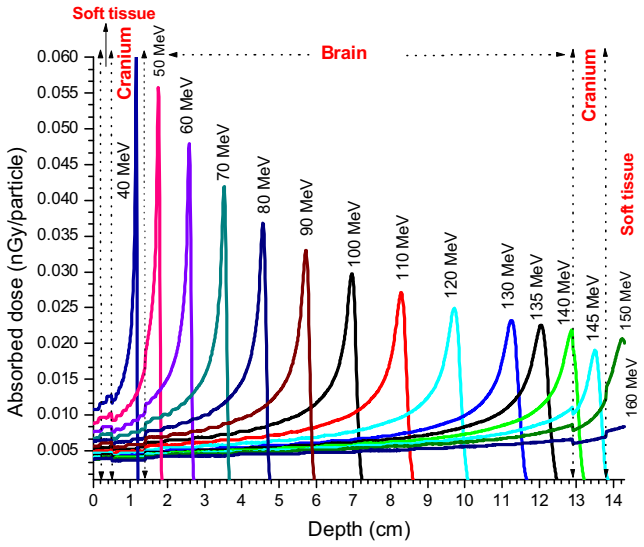

Fig. 2 – Pristine depth dose profiles in the slab head phantom for incident pencil beams with the energy range 40–145 MeV.

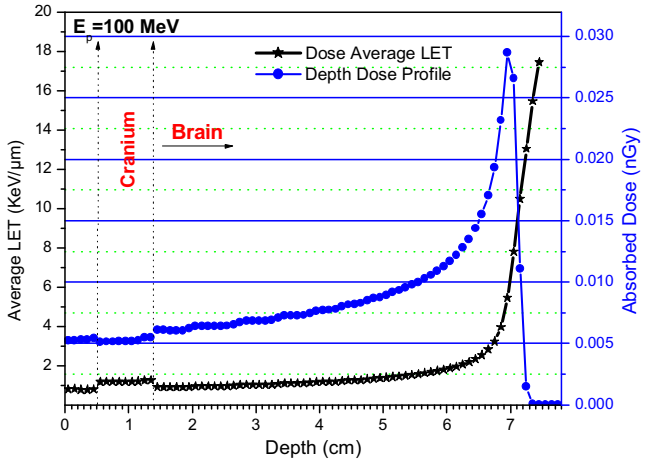

Fig. 3 – The absorbed depth dose profile and averaged LET for 100 MeV proton pencil beam.

all its remaining kinetic energy is deposited locally. We used the mesh tally type 3, and for some results the +F6 heating tally, to obtain volume-doses, or the depth dose profiles. By these tallies, the energy deposition by all charged particles, heavy nuclei, and energy deposited locally for particles created but not tracked, are scored. The mesh tally gives the energy deposition averaged over the volume, not the mass. Therefore, the mesh tally result should be divided by tissue densities to change the tally result to the dose.

4. Results and discussion

4.1. *Depth dose calculation*

The calculated results of depth dose profiles for proton beams with 10-MeV steps and energy range 40–160 MeV in the phantom are shown in Fig. 2. It can be seen that, for this arrangement, the Bragg peaks fall inside the brain. All energy and dose calculations were carried out until the errors shrank to less than 0.1%, achieved for about 2 million particles.

Depth dose profile and dose average linear energy transfer (LET) of 100 MeV proton beam are shown together in Fig. 3. LET increases with depth like absorbed dose and the upswing in the LET curve appears at a depth slightly greater than that of the dose curve and goes slightly beyond the dose peak. This is due to the fact that at the end of proton range, the average stopping power and, hence, the LET, increase as a result of decrease in the particle energy. On the other hand, some particles disappear in this region and, as a consequence, the dose, that is the product of particle fluence and stopping power divided by organ density, decreases, and the depth dose profile is in its distal region. This causes a very slight extension of the iso-effective dose beyond the physical dose.

We considered a typical tumor with the same composition of the brain tissue, spreading 2 cm inside the brain along the beam, with its center seated in a depth corresponding to the 100 MeV protons that means around 5 cm depth in the brain. Now, the goal is to come up with a flat dose region in the volume of interest. To achieve this, after establishing peak positions and range stragglings for different beam energies and proper fitting, appropriate beam energies that may cause an approximately flat dose distribution in the desired volume, were determined.[22] The energies ranged from 92.1 MeV to 108.0 MeV in 18 steps. The weight of each pristine depth dose profile was also obtained to create the SOBP in the depth of the tumor. On the basis of the calculated weight for each energy, one can say that the average proton energy is 103.6 MeV. The modulated profile with the modulation width of about 2 cm, along with the weighted pristine depth dose profiles, is shown in Fig. 4.

Characteristics of this profile, such as 95% modulation (M95) which is the distance between two points in proximal and distal regions where the dose falls to the 95% of 100% dose level, the (80–20%) penumbra that identifies the fall in the distal region, and a practical range in which the dose falls into 10% of 100% dose level, are shown in Fig. 4. These weighs were

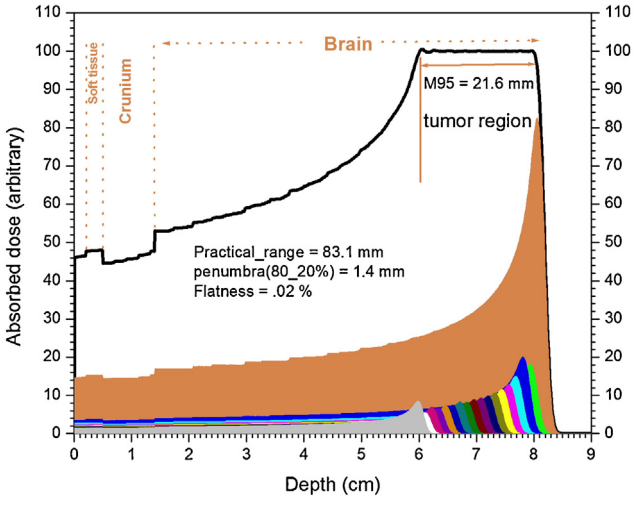

Fig. 4 – The expected SOBP profile along with all the weighted pristine depth dose profiles.

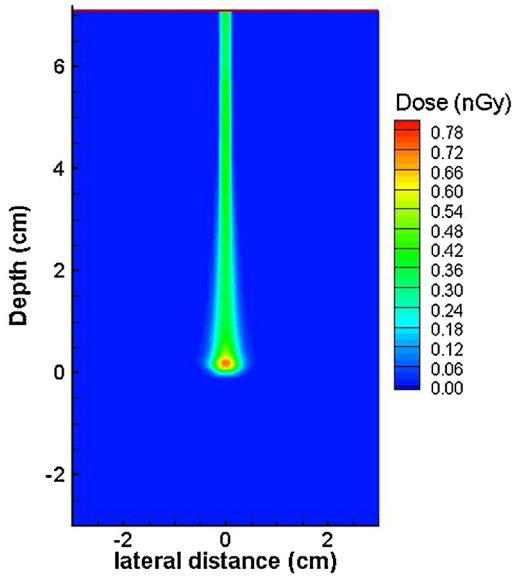

Fig. 5 – The 2D dose distribution contour for a 100 MeV proton pencil beam in a typical spot scanning system. The absorbed dose is in nGy.

implemented in the MCNPX input file to simulate and obtain the dose distribution in the phantom. The two dimensional (2D) dose distribution for a 100 MeV mono energetic proton beam, and the modulated profile are shown in Figs. 5 and 6, respectively, for a typical spot scanning system.

The role of the intensity modulated beam to spread out the Bragg peak longitudinally in the tumor volume is seen in Fig. 6. Indeed, by altering the beam energy with weighted intensity, one layer of the tumor is scanned each time. As

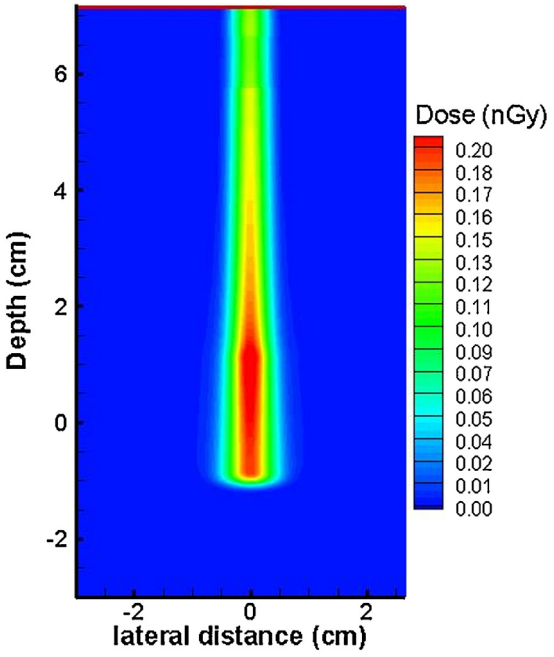

Fig. 6 – The 2D dose distribution contour for a modulated profile in a typical spot scanning system. The absorbed dose is in nGy.

mentioned before, the distance between neighboring layers should be chosen in proportion to the distal fall of the pristine profiles which depend on energy. This links the "layer-interval" to the modulation range position for a dynamical energy change in a spot scanning system. This, does not apply to passive scattering beam lines, or active beam lines that use an energy selection system (set of degraders) to adjust the beam energy; particles meet approximately the same tissue-equivalent-range, and experience a similar range straggling and, hence, all pristines have the same peak width. It is clear that to broaden the dose pattern laterally, the spot should move transversally in proportion to the lateral penumbra of the lateral dose profile.[24]

4.2. *Absorbed energy*

To evaluate the energy deposited in the brain region, monoenergetic proton pencil beams were considered to irradiate a slab head phantom. It was seen that beams with energies higher than 140 MeV lost part of their energies in the organs after the brain. Thus, it is expected that the energy deposit within the brain increases up to the maximum, as the energy of the incident beam is increased, and thereafter, due to protons penetrating the organs after the brain, starts to decline. In Fig. 7a the energy deposit in the brain region is shown. The 40 MeV proton beam is not able to penetrate the brain tissue, but for higher energies, the energy deposit in the brain increases until going beyond the energy of ~135 MeV, this is shown in Fig. 7b as percentage. At the optimum energy of ~135 MeV, there seems to be 89% of it deposited in the brain. Needless to say, these figures depend on the location of the tumor. For instance, if the tumor is located in the middle of the brain, say 5 cm deep inside, a 100 MeV beam would be required to place the Bragg peak at the same position; for this energy, the energy deposit within the brain is about 80%. From an earlier work of ours[22] and the result just quoted, one can conclude that with a 100 MeV proton pencil beam, a middle seated brain tumor with lateral dimensions of about 5 mm can be well targeted, and expect an energy deposition of 80% in the brain. For the aforementioned intensity modulated profile, an average of about 85.6 MeV (82.6%) of proton energy is deposited in the brain volume, out of which, 32.8 MeV is lost in the tumor.

For the SOBP profile of Fig. 4, on average, 32% of the proton energy is deposited in the tumor. For this profile, the peak-to-entrance ratio is 2.2, which is 2.7 times smaller than the corresponding value for the 100 MeV beam energy.

Fig. 8a shows the energy deposition within various tissues embedded in the slab head phantom, for proton pencil beams of 70, 100, 130 MeV, and also for the modulated profile. The percentage of deposited energy per source particle energy for the tissues is shown in Fig. 8b. It is seen that for beams with their Bragg peaks entirely inside the brain, the energy deposit in the brain increases with the beam energy, and for tissues located before (after) the brain, it decreases (increases).

The energy losses in the organs along the particle tracks are shown in Fig. 9 as functions of incident beam energies between 40 and 145 MeV. Fig. 10 shows the absorbed doses (nGy/particle) for various organs along the particle tracks versus the incident proton energy. It can be seen that by increasing the beam energy, the energy deposition in the

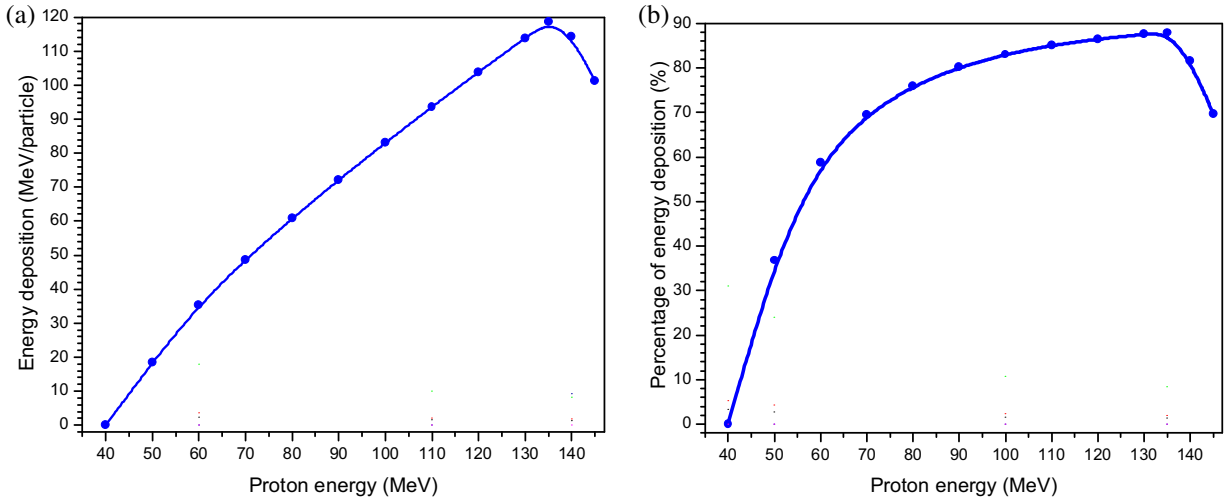

Fig. 7 – Variation of absorbed energy in brain, (a) absolute and (b) percentage; as functions of incident proton energy.

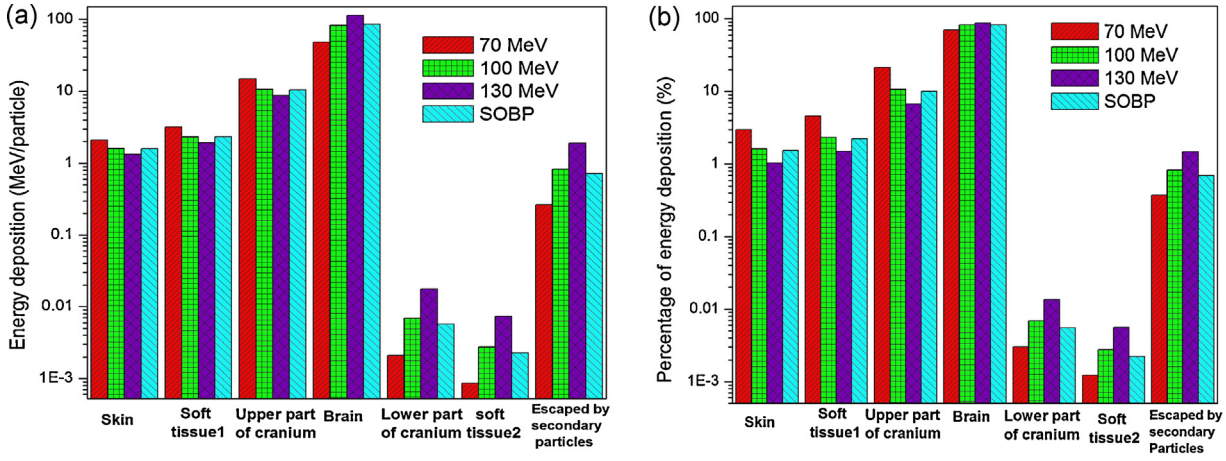

Fig. 8 – The absorbed energy (a) and percentage of the absorbed energy (b) in various tissues for three different beam energies and for the modulated profile along with the escaped energy by secondary particles.

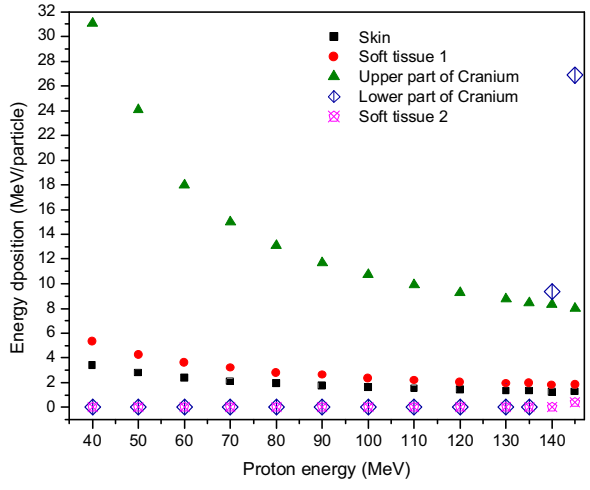

Fig. 9 – Absorbed energy in tissues located on proton beam tracks versus energy.

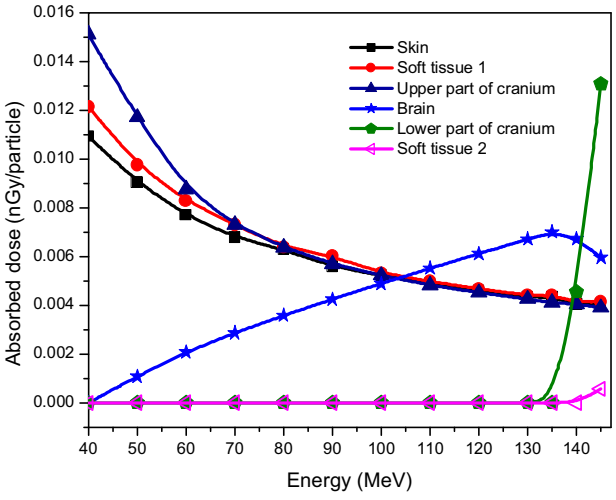

Fig. 10 – Absorbed doses in different tissues of slab head phantom as functions of incident proton energy.

organs located before the brain decreases. Especially, for upper part of the cranium this decrease in energy deposit is faster. At similar conditions, for organs located after the brain, the energy deposit does not show any noticeable change up to ~140 MeV. This confirms the role of protons in the treatment of deep-seated tumors.

4.3. *Production of secondary neutrons and photons*

Two most important secondary particles, i.e. neutrons and photons, were paid special attention to in this study. All "non-primary" particles are produced either by the interactions of the primary protons, or by the interactions of the secondary particles. In Fig. 11a and b the neutron and photon productions per primary protons are shown, respectively, as functions of proton energy. It is seen that by increasing beam energy, the production increases. Neutron and photon productions at $E_p = 40$ MeV, rise from 0.27% and 1.60%, respectively, to 10.14% and 9.10% at $E_p = 140$. For both curves, the calculated data are well fitted by quadratic functions whose constant parameters are given as legends in the figures

Fig. 12a shows the amount of energy escaped from the head by neutrons and photons, and Fig. 12b shows the same results in percentage. The quadratic function fitted to the neutron data is also given in Fig. 12b. While the escaped energy by secondary photons has small variations with the incident proton energy, this value for neutrons is strongly energy-dependent with respect to the incident proton energy, and goes from zero at 40 MeV to 2.44 at 145 MeV.

It is interesting to note that at all energies; the escaped energy by photons from the head phantom is approximately constant and about 0.10%. A closer look shows that it averages 0.16% with a standard deviation of 0.02%, whereas, for neutrons it changes from 0.02% at 40 MeV up to 1.68% at 145 MeV. Thus, we can conclude that for proton beams with energies of 60 MeV and higher, the escaped energy by secondary neutrons is larger than that of secondary photons. For high beam energies of around 120 MeV, the fraction of energy that escapes by neutrons is almost 10 times greater than that of photons, and even becomes greater for higher proton energies. This justifies the vast number of studies and publications on secondary neutrons compared to secondary photons.[6,7,9,11,15,25,28] The

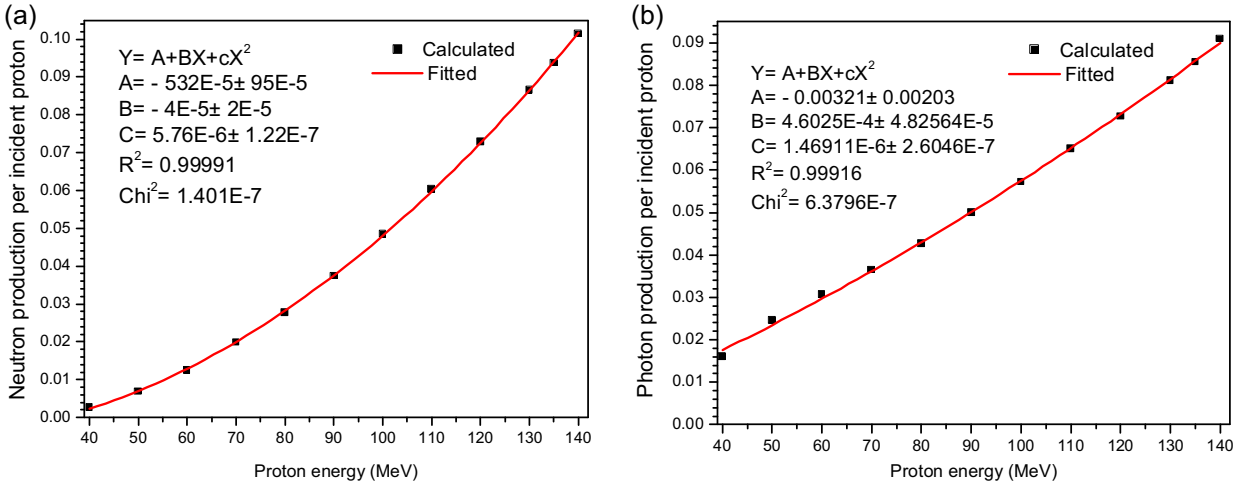

Fig. 11 – Secondary particle production per source proton, versus proton beam energy: (a) neutron and (b) photon.

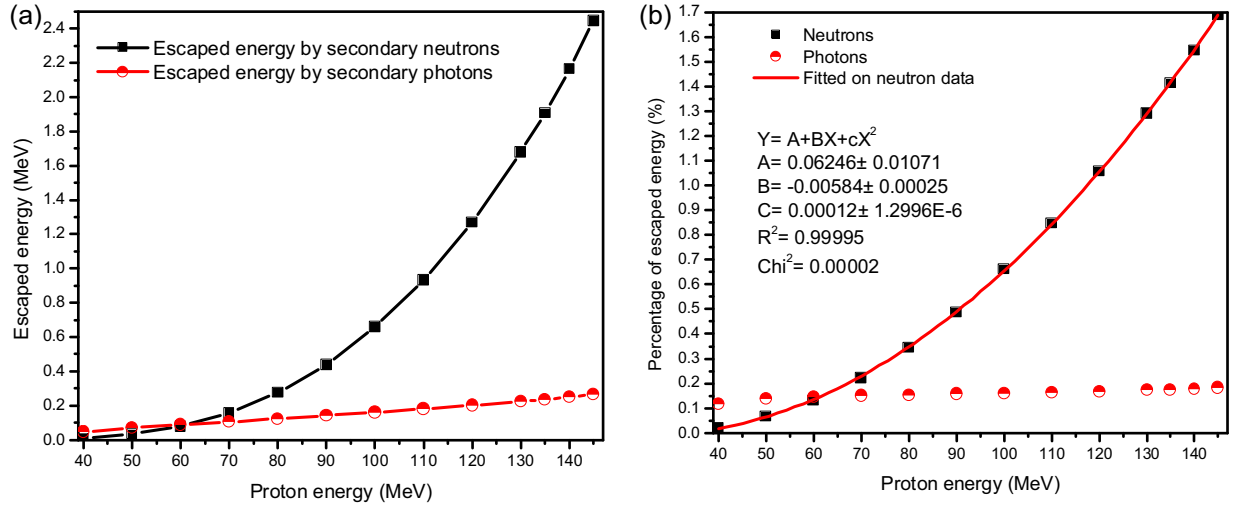

Fig. 12 – (a) Escaped energy by secondary neutrons and photons per source proton versus the energy of proton beam; (b) Relative escaped energy by secondary neutrons and photons per source proton versus the energy of proton beam.

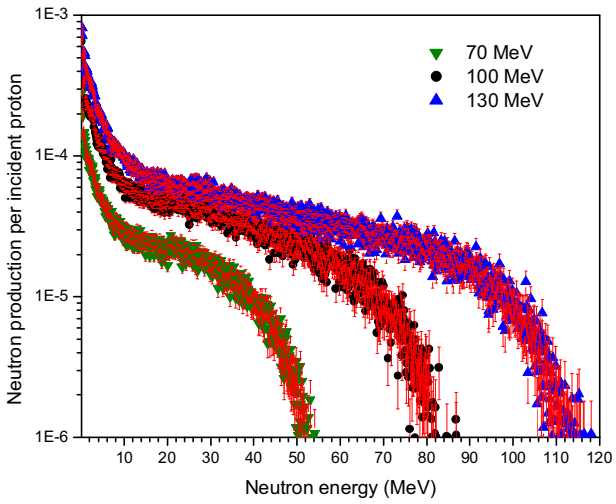

Fig. 13 – Neutron spectra produced by three different beam energies of 70, 100 and 130 MeV.

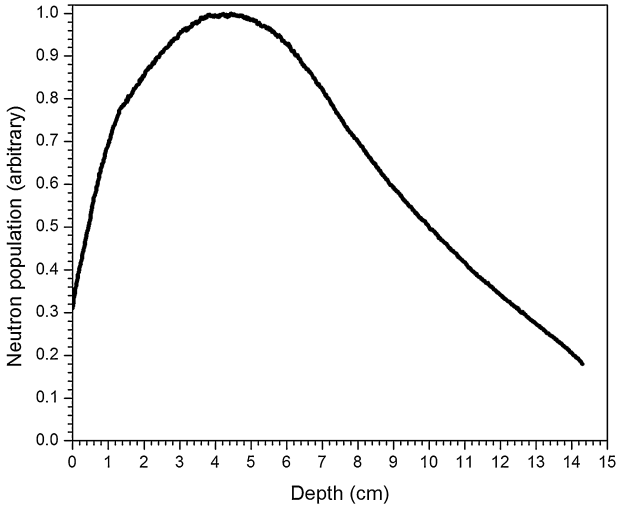

Fig. 15 – Neutron population as a function of depth in the head phantom.

overall fraction of proton energy that escapes by secondary neutrons and photons, range from 0.14% to 1.86% for incident proton beam-energy range 40–145 MeV. At energy of 110 MeV, this figure is about 1.00%. For the modulated profile, neutron and photon productions are 4.9% and 7.3%, respectively. Here, the energy escape by neutrons is 0.53%, and 0.19 for photons.

Fig. 13 shows the energy spectra of neutrons produced per incident proton for three different beam energies of 70, 100 and 130 MeV. It is seen that the neutron spectra have relatively large peaks at low energies; however, the spectra tail to high energies with smaller intensities. Fig. 14 also shows the energy spectrum of photon produced a 100 MeV incident proton. The characteristic photon energies due to nuclear transitions of radioactive atomic nuclei produced in the interactions, mostly by the primary protons or other secondary particles produced in the tissue, are illustrated in the figure.

The maximum non-elastic nuclear cross-section occurs at about 10–50 MeV.[29] Thus, it is expected to see a maximum for secondary particle population in the depth corresponding to 10–50 MeV, as shown for neutrons in Fig. 15. Since the peaks

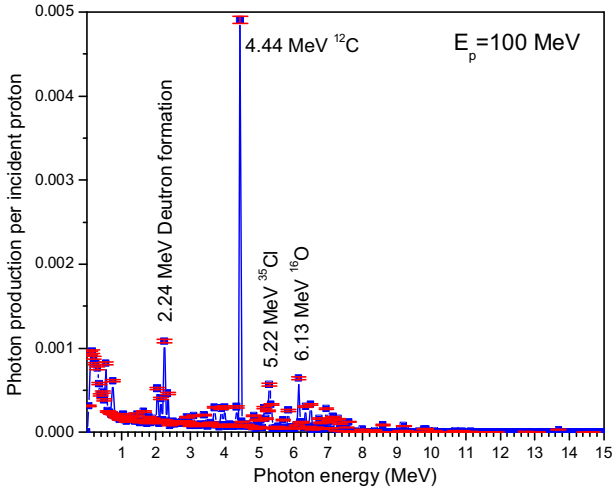

Fig. 14 – Spectrum of photons produced by 130 MeV beam energy.

appear when protons come to about 5–8 MeV, the maximum in the secondary population occurs just before the Bragg peak.

Substituting the phantom with a water tank of the same dimensions, it is clear that the depth dose profiles affect as a result of different composition and density. Using a water tank, instead of the detailed phantom and for the tumor specified in Fig. 4, the whole energy that escapes from the treatment volume by secondary particles and goes to a region far from it, decreases approximately 0.2 MeV. It is clear that for tumors seated deeper in the brain, the difference would be more than this value.

5. Conclusion

For the geometry of our choice, and proton pencil beams of ~40–140 MeV, the Bragg peaks fall inside the brain tissue. A typical SOBP profile is created using proper mono energetic proton pencil beams with their relevant weights. A 2D-intensity modulated dose distribution for a single spot is obtained, and the portion of energy that is deposited in the tumor is calculated. Energy deposition increases to a maximum value of about 90% at 135 MeV. Energy depositions and absorbed doses in different tissues located before and after the brain were calculated. We obtained quadratic functions with appropriate parameters for both neutron and photon secondary production. The fraction of energy escaped by photons is approximately constant for all energies and has a mean value of 0.16%, while for neutrons it changes as a quadratic function of beam energy from 0.02% up to 1.68%. Our MC results show that the escaped energy by neutrons at 145 MeV incident proton beam is 2.44 MeV. It is shown that for high-energy proton beams, most of the escaped energy from the head is due to secondary neutrons. For instance, at about 120 MeV, the energy escaped by secondary neutrons is almost 10 times greater than that of photons. The overall fraction of proton energy that escapes by secondary neutrons and photons is approximately 1% for incident proton beam of 110 MeV, and 1.86% for 145 MeV protons.

Conflict of interest

None declared.

Financial disclosure

None declared.

REFERENCES

1. Haberer T. Advances in charged particles therapy. In: *Nuclear physics in 21st century: Int. Nucl. Phys. Conf. INPC 2001. AIP Conf. Proc., vol. 610*. 2002. p. 157–66.
2. Perez CA, Mutic S. Advances and future of radiation oncology. *Rep Prac Oncol Radiother* 2013;**I8**:329–32.
3. Kraft G. Tumor therapy with heavy charged particles. *Prog Part Nucl Phys* 2000;**45**:S473–544.
4. Zietman A. Proton beam and prostate cancer: an evolving debate. *Rep Prac Oncol Radiother* 2013;**I8**:339–42.
5. Taddei PJ, Markovic D, Fontenot JD, et al. Stray radiation dose and second cancer risk for a pediatric patient receiving craniospinal irradiation with proton beams. *Phys Med Biol* 2009;**54**:2259–75.
6. Jiang H, Wang B, Xu XG, Suit HD, Paganetti H. Simulation of organ specific patient effective dose due to secondary neutrons in proton radiation treatment. *Phys Med Biol* 2005;**50**:4337–53.
7. Polf JC, Newhauser WD, Titt U. Patient neutron dose equivalent exposures outside of the proton therapy treatment field. *Radiat Prot Dosim* 2005;**115**:154–8.
8. Xu XG, Bednarz B, Paganetti H. A review of dosimetry studies on external beam radiation treatment with respect to second cancer induction. *Phys Med Biol* 2008;**53**:R193–241.
9. Jarlskog CZ, Lee C, Bolch W, Xu XG, Paganetti H. Assessment of organ specific neutron doses in proton therapy using whole-body age-dependent voxel phantoms. *Phys Med Biol* 2008;**53**:693–714.
10. Agosteo S, Birattari C, Caravaggio M, Silari M, Tosi G. Secondary neutron and photon dose in proton therapy. *Radiother Oncol* 1998;**48**:293–305.
11. Brenner DJ, Hall EJ. Secondary neutron in clinical proton radiotherapy: a charged issue. *Radiother Oncol* 2008;**86**:165–70.
12. Kim S, Byung JM, Yoon M, et al. Secondary radiation doses of intensity-modulated radiotherapy and proton beam therapy in patient with lung and liver cancer. *Radiother Oncol* 2011;**98**:335–9.
13. National Research Council of the National Academies. *Health risks from exposure to low levels of ionizing radiation – BEIR VII*. Washington, DC: The National Academies Press; 2006.
14. Kellerer A, Rossi H. A generalized formulation of dual radiation action. *Radiat Res* 1978;**75**:471–88.
15. Joiner MC, Field SB. The response of mouse skin to irradiation with neutrons from the 62 MeV cyclotron at Clatterbridge, UK. *Radiother Oncol* 1988;**12**:153–66.
16. Slopsema R. Beam delivery using passive scattering. In: Paganetti H, editor. *Proton therapy physics*. Boca Raton: CRC Press/Taylor & Francis; 2011. p. 125–56.
17. Paganetti H. Dose to water versus dose to medium in proton beam therapy. *Phys Med Biol* 2009;**54**:4399–421.
18. Torfimov A, Borfeld T. Beam delivery sequencing for intensity modulated proton therapy. *Phys Med Biol* 2003;**48**:1321–31.
19. ICRU, International Commission on Radiation Units and Measurements. Report 46: photon, electron, proton, and neutron interaction data for body tissues. *J ICRU* 1992.
20. Eckerman KF, Cristy M, Ryman JC. *The ORNL mathematical phantom series*; 1996. Available at: http://homer.ornl.gov/vlab/mird2.pdf
21. Kooy HM, Clasie BM, Lu HM, et al. A case study in proton pencil-beam scanning delivery. *Int J Radiat Oncol Biol Phys* 2010;**76**:624.
22. Pedroni E, Bacher R, Blattmann H, et al. The 200 MeV proton therapy project at the Paul Scherrer Institute: conceptual design and practical realisation. *Med Phys* 1995;**22**(1):37–53.
23. Haberer Th Becher W, Schardt D, Kraft G. Magnetic scanning system for heavy ion therapy. *Nucl Instrum Methods Phys Res A* 1993;**330**:296–305.
24. Jia SB, Mowlavi AA, Hadizadeh MH, Ebrahimi Looshab M. Range straggling and multiple scattering effects on brain proton therapy. *Int J Radiat Res* 2014 (in press).
25. Schneider U, Agosteo S, Pedroni E, Besserer J. Secondary neutron dose during proton therapy using spot scanning. *Int J Radiat Oncol Biol Phys* 2002;**53**(1):244.
26. Waters LS, Hendricks J, McKinney G. *MCNPX, Monte Carlo N-particle transport code system for multiparticle and high energy applications*. Los Alamos, NM: Los Alamos National Laboratory; 2002.
27. Pelowitz DB, editor. *MCNPXTM user's manual, version 2.6.0*. Los Alamos, NM: Los Alamos National Laboratory; 2008. LA-CP-07-1473.
28. Pérez-Andújar A, Newhauser WD, DeLuca PM. Neutron production from beam-modifying devices in a modern double scattering proton therapy beam delivery system. *Phys Med Biol* 2009;**54**:993–1008.
29. ICRU, International Commission on Radiation Units and Measurements. Report 63: nuclear data for neutron and proton radiotherapy and for radiation protection. *J ICRU* 2000.